Raman study of alloy potential fluctuations in $Mg_xZn_{1-x}O$ nanopowders

2007 J. Phys.: Condens. Matter 19 186201

(http://iopscience.iop.org/0953-8984/19/18/186201)

IOP PUBLISHING JOURNAL OF PHYSICS: CONDENSED MATTER

J. Phys.: Condens. Matter **19** (2007) 186201 (8pp) doi:10.1088/0953-8984/19/18/186201

Raman study of alloy potential fluctuations in $Mg_xZn_{1-x}O$ nanopowders

Ching-Ju Pan, Kuo-Feng Lin, Wei-Tse Hsu and Wen-Feng Hsieh[1]

Department of Photonics and Institute of Electro-Optical Engineering, National Chiao Tung University, 1001 Tahsueh Road, Hsinchu 30050, Taiwan, Republic of China

E-mail: wfhsieh@mail.nctu.edu.tw

Received 25 December 2006, in final form 26 February 2007
Published 4 April 2007
Online at stacks.iop.org/JPhysCM/19/186201

Abstract

The blueshift of near-band-edge emission and excitonic absorption indicate that Zn^{2+} ions are successfully substituted by Mg^{2+} ions in $Mg_xZn_{1-x}O$ nanopowders for $0 \leqslant x \leqslant 0.14$. The changes in Raman spectral linewidth and the asymmetry of the E_2 (high) mode for various Mg contents can be well described by a modified spatial correlation model that considers the grain size distribution. With increasing Mg concentration, the alloy potential fluctuations lead to a decrease in the grain size, which is induced by the surplus Mg^{2+} that could form MgO clusters surrounding the crystalline MgZnO.

1. Introduction

Among wide-band-gap semiconductor materials, a pronounced advantage for ZnO (3.37 eV) is its large exciton binding energy (∼60 meV) [1], so it has been recognized as a promising candidate to compete with GaN for the development of short-wavelength photonic devices, such as ultraviolet detectors, light-emitting diodes, and laser diodes. To fully utilize ZnO-based technologies, band gap engineering and p-type doping are still remaining issues in modern optoelectronics. Fabrication and characterization of alloys such as (Mg, Zn)O and (Cd, Zn)O have been proved feasible to realize the band gap modulation of ZnO. MgZnO can be used as energy barrier layers of ZnO light-emitting devices and $ZnO/Mg_{0.2}Zn_{0.8}O$ coaxial nanorod single quantum well structures for carrier confinement [2, 3]. Additionally, Jingbo *et al* [4] proposed that, using first-principles band-structure calculations, the p-type dopability of ZnO was achieved by lowering the ionization energy of acceptors in ZnO by codoping acceptors with donor or isovalent atoms (e.g., Mg or Be). Therefore, the structural and optical properties of MgZnO alloys have attracted significant coverage [5–9].

The wurtzite structure of ZnO belongs to the space group C_{6v}^4. Group theory predicts the existence of the following optic phonon modes: $A_1 + 2B_1 + E_1 + 2E_2$ at the Γ point of the

[1] Author to whom any correspondence should be addressed.

Brillouin zone; where A_1 and E_1 modes are both Raman and infrared active, and B_1 (low) and B_1 (high) modes are silent. However, the nonpolar E_2 modes are Raman active and have two frequencies: E_2 (high) is related to the vibration of oxygen atoms and E_2 (low) is related to the Zn sublattice. Recently, considerable attention has been devoted to the compositional dependence of the line shape (i.e., linewidth and asymmetry) of wurtzite E_2 phonons using the spatial correlation (SC) model [10, 11]. For example, Beserman *et al* [12] have discussed the asymmetric behaviour of the E_2 Raman linewidth of $Al_xGa_{1-x}N$ alloys attributed to the activation of phonons of $q \geqslant 0$ arising from the disorder of the alloys. Wang *et al* [13], who studied $Zn_{1-x}Mn_xO$, have observed that the substitutional disorder can introduce changes in the spectral line position, linewidth, and asymmetry of the first-order E_2 (high) phonon mode. However, there are no reports to our knowledge on compositional disorder related to the line shape of E_2 phonons in $Mg_xZn_{1-x}O$ systems. Here, we present the first step to provide a detailed investigation with the SC model on the influence of the first-order Raman spectra in $Mg_xZn_{1-x}O$ nanopowders, concentrating on the E_2 (high) mode.

In this paper, we report on the preparation of $Mg_xZn_{1-x}O$ nanopowders on sapphire substrates using a sol–gel method. By adjusting the Mg compositions within the range of $0 \leqslant x \leqslant 0.14$, obvious blueshifts in the absorption and photoluminescence (PL) spectra were observed. Additionally, the broadening and asymmetry of the E_2 (high) spectral line by using micro-Raman spectroscopy shows good agreement with the modified SC model that is based on the finite correlation length of a propagating phonon, due to the alloy potential fluctuations (APFs) and grain size distribution (GSD).

2. Experimental details

MgZnO nanopowders were synthesized by the following procedure. Stoichiometric zinc acetate dihydrate (99.5% $Zn(OAc)_2{\cdot}2H_2O$, Riedel-deHaen) and magnesium acetate tetrahydrate (99.5% $Mg(OAc)_2{\cdot}4H_2O$, Riedel-deHaen) were individually dissolved into diethylene glycol (99.5% DEG, ethylenediamine-tetra-acetic acid (EDTA)) to make 0.1 M solutions. The resultant solutions were put separately in a centrifuge operating at 3000 rpm for 30 min, and transparent solutions were obtained containing dispersed single-crystalline ZnO and MgO nanocrystals, respectively. Next, we mixed the supernatant solutions of ZnO and MgO nanocrystals with desired volume fractions, which were dropped onto sapphire (0001) substrates and dried at 150 °C. The Mg contents were controlled by varying the volume ratio of MgO- and ZnO-supernatant solutions from 0–40%. Finally, all the samples were annealed in a furnace at 900 °C under air atmosphere for 1 h, then slowly cooled down to room temperature.

The morphology of MgZnO nanopowders was characterized by field-emission scanning electron microscopy (FESEM, JEOL-2100F). The PL measurement was made using a 20 mW He–Cd laser at wavelength of 325 nm and the emission light was dispersed by a TRIAX-320 spectrometer and detected by a UV-sensitive photomultiplier tube. Optical absorption spectra were recorded on the same spectrophotometer with a deuterium lamp. Micro-Raman spectroscopy was carried out using Ar^+ laser ($\lambda = 488$ nm) with power of 40 mW as the pump source, and a SPEX 1877C triple-grating spectrograph equipped with a liquid-nitrogen-cooled CCD at 140 K.

3. Results and discussion

3.1. Surface morphology and optical properties

Figure 1 presents an SEM image of the powders; the average crystallite size is ∼150 nm, which does not reveal a quantum size effect (the Bohr radius of excitons in ZnO ∼2.34 nm).

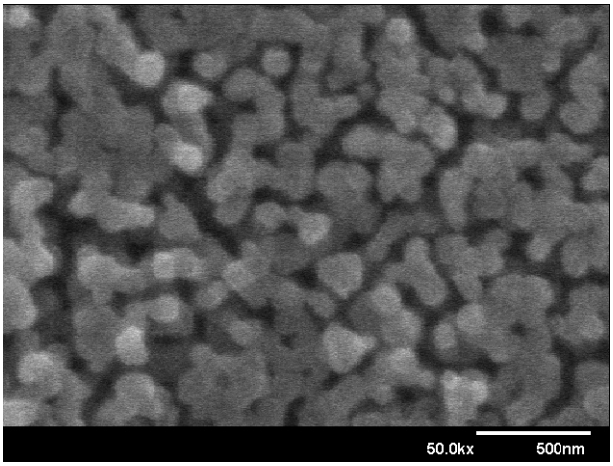

Figure 1. The SEM image of the 10.9% Mg sample.

Shown in figure 2(a) are the photoluminescence (PL) and absorption spectra taken at room temperature of five annealed samples having volume ratios of MgO/ZnO equal to 0, 6, 10, 20, and 40%, respectively. All of the PL spectra were dominated by highly efficient near-band-edge (NBE) emission, which originates from free-exciton emission and its replicas [14–16]. The luminescence shows a Stokes shift to the lower-energy side of the absorption edge, which is frequently familiar in alloy semiconductors, where carriers feel different potentials depending on the local concentration or arrangement of the substituting elements. This effect is larger in ZnO than in III–V materials, because the Bohr radius of the exciton in ZnO is smaller and the exciton is more sensitive to local inhomogeneity [17]. Moreover, the excitonic transition energy exhibits a blueshift of ∼0.24 eV as the volume ratio of MgO/ZnO increases from 0 to 40%. Similar indications can be seen clearly in the absorption spectra, showing a blueshift from 3.33 to 3.56 eV with increasing MgO content. Namely, Mg doping causes a band-gap enlargement of ∼240 meV.

Based on the formula $E(\mathrm{Mg}_x\mathrm{Zn}_{1-x}\mathrm{O}) = E(\mathrm{ZnO}) + 1.64 * x$ (eV), the Mg content in the $\mathrm{Mg}_x\mathrm{Zn}_{1-x}\mathrm{O}$ thin films has been determined for $0 \leqslant x \leqslant 0.2$, grown by pulsed laser deposition [18]. Here, $E(\mathrm{Mg}_x\mathrm{Zn}_{1-x}\mathrm{O})$ and E (ZnO) are the NBE emission peak positions of $\mathrm{Mg}_x\mathrm{Zn}_{1-x}\mathrm{O}$ and ZnO, respectively. The Mg contents in each of our five alloys, with volume ratios of MgO/ZnO equal to 0, 6, 10, 20, and 40%, were calculated to be 0, 6, 11, 13, and 14%, respectively. Figure 2(b) illustrates the evaluated Mg content of the nanopowders as a function of the volume ratio of MgO/ZnO. The result reveals that MgO has a solubility limit of above 10% in ZnO, in accordance with the present synthesized approach. This tendency closely coincides with that reported for $\mathrm{Mg}_x\mathrm{Zn}_{1-x}\mathrm{O}$ fabricated by a solution-based route, in which MgO did not completely dissolve with ZnO for $x > 0.1$ [19]. Therefore, the UV emission and absorption exhibits a progressive blueshift with initially increasing MgO content until $x = 0.1$ or MgO/ZnO(= 0.1:1), demonstrating that Mg^{2+} is incorporated into the ZnO lattice and occupies the lattice sites of Zn^{2+}; thereafter, it tends to slowly blueshift with increasing MgO content, which implies that Mg^{2+} is no longer completely incorporated into the ZnO lattice.

3.2. Raman scattering spectra

To investigate the influence of Mg doping on the microscopic structures and the vibrational properties, the micro-Raman spectra of the five samples were measured in a backscattering

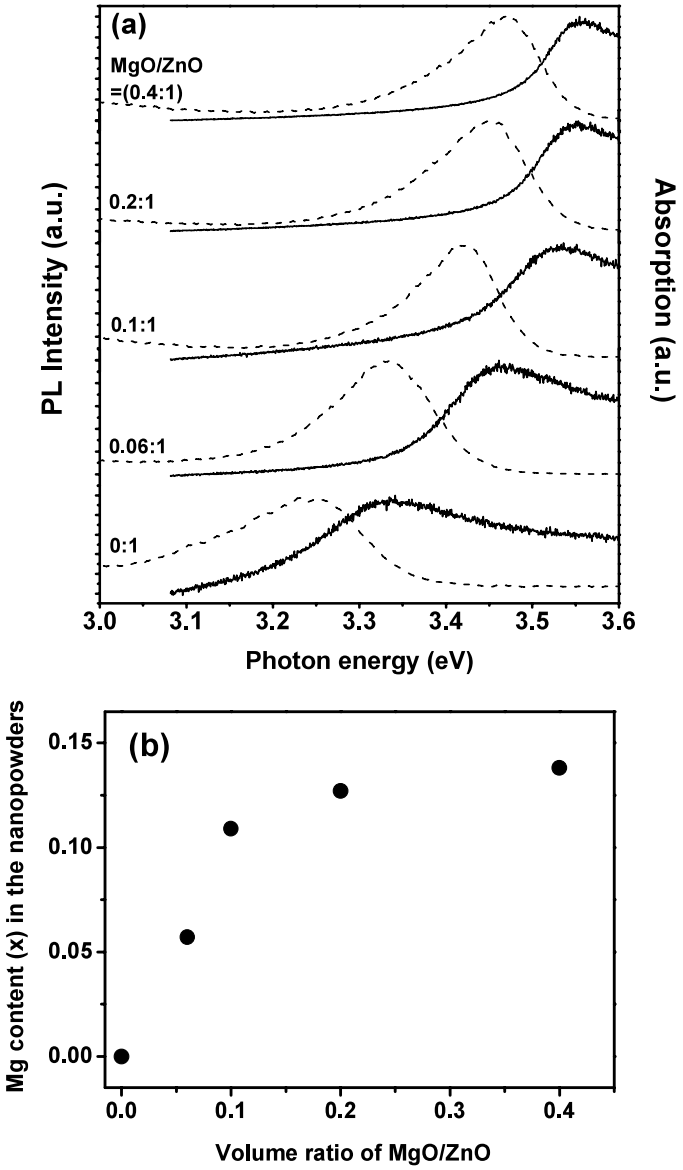

Figure 2. (a) Photoluminescence (solid curves) and absorption (dashed curves) spectra of $Mg_xZn_{1-x}O$ alloys for different MgO/ZnO volume ratios. (b) The calculated Mg content in the $Mg_xZn_{1-x}O$ nanopowders as a function of the MgO/ZnO volume ratio.

configuration with a fixed laser spot of about 2 μm^2, as shown in figure 3 with the inverse x-sequence compared to that in figure 2(a). We found the spectral peaks at 438, and 584 cm^{-1} of pure ZnO nanopowders which originate from E_2 (high) and E_1 (LO), respectively. The assignments of the Raman peaks have been reported previously [20–22]. Furthermore, it is interesting to note that the line shape of the E_2 (high) phonon at around 438 cm^{-1} depends considerably on the Mg incorporation.

In alloy semiconductors, the phonons can be spatially confined, owing to either the potential fluctuations of the alloy disorder or finite crystallinity, which gives rise to a relaxation

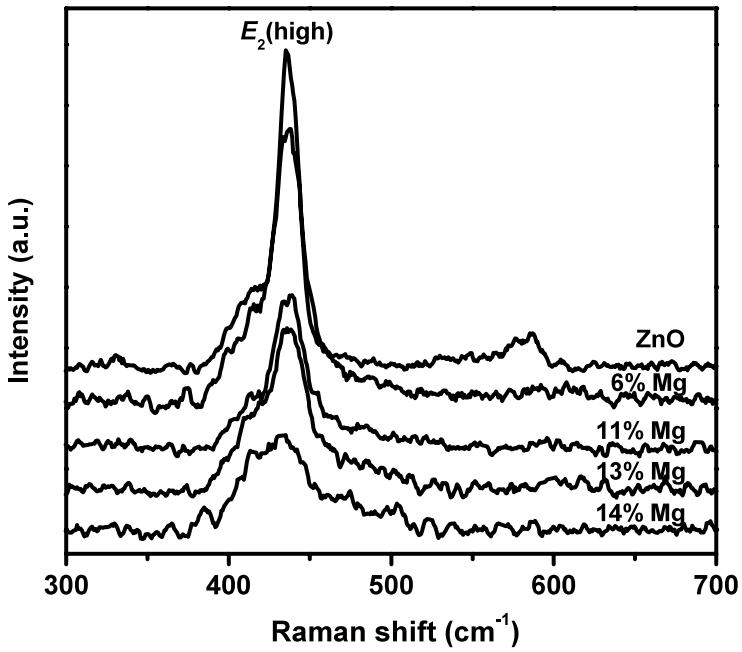

Figure 3. Micro-Raman spectra of $Mg_xZn_{1-x}O$ nanopowders with various Mg contents.

of the $q = 0$ selection rule in Raman scattering [22–24]. Therefore, the spatial correlation length of phonon in alloys becomes finite. The localized phonon mode will lead to the shift and asymmetric broadening of the Raman line shape. Several groups [13, 25–27] have found these phenomena in ZnO system doped with N, Mn, and Co elements.

The spatial phonon confinement could arise from APFs, as Mg^{2+} random substitution induces microscopic structural disorder in the periodic zinc atomic sublattice and breaks the translational symmetry. Besides, Islam *et al* [28] and Lin *et al* [29] proposed that the crystallite size distribution could affect the shifts of Raman frequencies and line shapes as well in Si and ZnO nanostructures. Therefore, they modified the Raman spectral intensity expression of the SC model by introducing a Gaussian crystallite size distribution (CSD) of an ensemble of spherical crystallites with mean crystallite size L_o and standard deviation σ. It can be written as

$$I(\omega) \propto \int_0^1 \frac{f(q)q^2 \exp(-q^2L_o^2/4)\,\mathrm{d}q}{[\omega - \omega(q)]^2 + (\Gamma/2)^2},$$

where q is presented in units of $2\pi/a$, a is the lattice constant, $\omega(q)$ is the phonon dispersion relation, Γ is the linewidth of the E_2 (high) phonon in the bulk ZnO, and $f(q) = 1/\sqrt{1 + q^2\sigma^2/2}$ is the characteristics of the CSD. Setting L_o and σ as adjustable parameters to fit with the experimental data, we calculated normalized Raman profiles of $Mg_xZn_{1-x}O$ nanopowders to depict the Raman line-shapes of the E_2 (high) band; they are plotted in figure 4(a). The solid line represents the theoretical fits of the modified SC model, and the open dots are the experimental data. The L_o values decrease with increasing Mg composition, corresponding to 17, 13.5, 12.5, and 9 nm for $x \sim 6$, 11, 13, and 14%, respectively; nevertheless, the changes of $\dot{\sigma}$ and asymmetry Γ_a/Γ_b are reversed.

It is understandable that further Mg^{2+} incorporated into the ZnO lattice results in the increment of microscopic substitutional disorder, and hence enhances the standard deviation

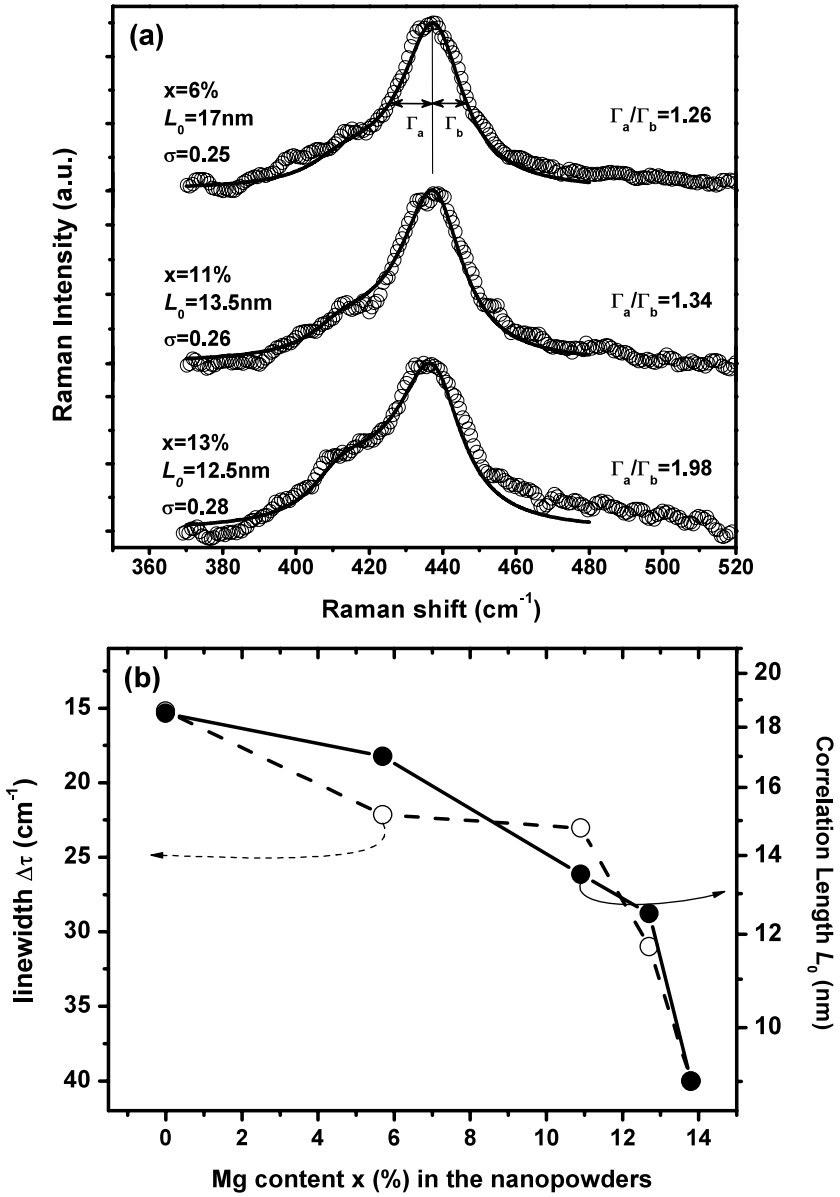

Figure 4. (a) Experimental and calculated line shapes of the E_2 (high) band for $Mg_xZn_{1-x}O$ nanopowders with $x = 6\%$, 11%, and 13%. The corresponding correlation length L_o, standard deviation σ and asymmetric broadening Γ_a/Γ_b are also labelled. (b) Linewidth $\Delta\tau$ and correlation length L_o of the E_2 (high) phonon as a function of Mg concentration.

σ and asymmetrical line shape ($\Gamma_a > \Gamma_b$). In $Mg_xZn_{1-x}O$ alloy semiconductors, the correlation length L_o of the E_2 (high) phonon can be interpreted as the average size of the localized regions [24]; thus, the phonon-extended region becomes smaller with increasing Mg content. Accordingly, the localized regions stand for microstructural geometries resulting from sublattice disorder, microcrystallite size or structural damage [23]. Similarly, the Raman spectral position and linewidth $\Delta\tau$ can also be obtained by the fitting the spectral intensity

using the modified spatial correlation mode, in which the E_2 (high) phonon lines are slightly redshifted and remarkably broadened from 15.2 to 40 cm^{-1} (full width at half maximum, FWHM) as the Mg concentration in the $Mg_xZn_{1-x}O$ nanopowders is increased from $x = 0$ to 0.14.

Figure 4(b) reveals that the E_2 (high) phonon linewidth $\Delta\tau$ and the correlation length L_o are strongly correlated with the Mg content and vary drastically above $x \sim 0.1$. As also revealed in figure 2(b), the actual dopant of Mg above $x \sim 0.1$ was out of proportion to the volume ratio of MgO/ZnO. Hence, instead of being incorporated into the ZnO lattice, the excess Mg^{2+} could form MgO clusters surrounding the crystalline MgZnO, which leads to a decrease in the grain size. Namely, the spherical-shaped particles of ∼150 nm, as observed in SEM, are polycrystals formed by the agglomeration of much smaller crystalline subcrystals similar to those shown in the TEM images of Cheng *et al* [30]. Note that there is no significant blueshift of absorption and NBE emission due to the quantum size effect for crystal size larger than 7.4 nm [31]; hence, the blueshift of our MgZnO nanopowders is still dominated by the Mg incorporation. Therefore, the L_o and σ values are appropriate parameters accounting for the disorder due to the APFs and GSD of $Mg_xZn_{1-x}O$ alloys. Consequently, we would suggest that the APFs result in the change of the grain size with Mg substitution; for $x > 0.1$, the grain size diminishes as a result of the random distribution of aggregated Mg^{2+} ions in ZnO crystal lattice to form MgO clusters or nanocrystals, which partition a larger MgZnO crystal (e.g., ∼17–13.5 nm) into subcrystals ($\leqslant$9 nm).

4. Conclusion

We have synthesized $Mg_xZn_{1-x}O$ nanopowders with various Mg contents of $0 \leqslant x \leqslant 0.14$ by the sol–gel method. The room-temperature near-band-edge photoluminescence and absorption spectra are shown to be tuned by ∼0.24 eV towards the UV range upon more Mg substitution. In Raman-scattering studies, the microscopic nature of the substitutional disorder is discussed by analysing the compositional dependence of the E_2 (high) phonon mode in $Mg_xZn_{1-x}O$ alloys. It is shown that the Raman spectral broadening and asymmetry induced by the APFs can be quantitatively explained in terms of the modified SC model, considering the GSD. With increasing Mg concentration, the APFs lead to a decrease in grain size, which arises from the surplus Mg^{2+} that could form MgO clusters surrounding the crystalline MgZnO.

Acknowledgments

This work was partially supported by the National Science Council and the Ministry of Economic of the Republic of China under Contract no NSC-95-2745-M-009-002.

References

[1] Hümmer K 1943 *Phys. Status Solidi* b **56** 249
[2] Lim J H, Kang C K, Kim K K, Park I K, Hwang D K and Park S J 2006 *Adv. Mater.* **18** 2720
[3] Bae J Y, Yoo J and Yi G C 2006 *Appl. Phys. Lett.* **89** 173114
[4] Li J, Wei S H, Li S S and Xia J B 2006 *Phys. Rev.* B **74** 081201
[5] Ohtomo A, Kawasaki M, Koida T, Masubuchi K, Koinuma H, Sakurai Y, Yoshida Y, Yasuda T and Segawa T 1998 *Appl. Phys. Lett.* **72** 2466
[6] Schmidt R, Rheinlander B, Schubert M, Spemann D, Butz T, Lenzner J, Kaidashev E M, Lorenz M, Rahm A, Semmelhack H C and Grundmann M 2003 *Appl. Phys. Lett.* **82** 2260
[7] Ma J G, Liu Y C, Shao C L, Zhang J Y, Lu Y M, Shan D Z and Fan X W 2005 *Phys. Rev.* B **71** 125430
[8] Peng W Q, Qu S C, Cong G W and Wang Z G 2006 *Appl. Phys. Lett.* **88** 101902

[9] Suchand Sandeep C S, Philip R, Satheeshkumar R and Kumar V 2006 *Appl. Phys. Lett.* **89** 063102
[10] Richter H, Wang Z P and Ley L 1981 *Solid State Commun.* **39** 625
[11] Campbell I H and Fauchet P M 1986 *Solid State Commun.* **58** 739
[12] Bergman L, Bremser M D, Perry W G, Davis R F, Dutta M and Nemanich R J 1997 *Appl. Phys. Lett.* **71** 2157
[13] Wang J B, Zhong H M, Li Z F and Lu W 2005 *J. Appl. Phys.* **97** 086105
[14] Hsu H C, Tseng Y K, Chang H M, Kuo J H and Hsieh W F 2004 *J. Cryst. Growth* **261** 520
[15] Zhang B P, Binh N T, Segawa Y, Kashiwaba Y and Haga K 2004 *Appl. Phys. Lett.* **84** 586
[16] Hsu H C, Cheng C S, Chang C C, Yang S, Chang C S and Hsieh W F 2005 *Nanotechnology* **16** 297
[17] Zimmermann R 1990 *J. Cryst. Growth* **101** 346
[18] Lorenz M, Kaidashev E M, Rahm A, Nobis Th, Lenzner J, Wagner G, Spemann D, Hochmuth H and Grundmann M 2005 *Appl. Phys. Lett.* **86** 143113
[19] Tomar M S, Melgarejo R, Dobal P S and Katiyar R S 2001 *J. Mater. Res.* **16** 903
[20] Wang R P, Xu G and Jin P 2004 *Phys. Rev.* B **69** 113303
[21] Chen S, Liu Y, Shao C, Mu R, Lu Y, Zhang J, Shen D and Fan X 2005 *Adv. Mater.* **17** 586
[22] Xing Y J, Xi Z H, Xue Z Q, Zhang X D, Song J H, Wang R M, Xu J, Song Y, Zhang S L and Yu D P 2003 *Appl. Phys. Lett.* **83** 1689
[23] Parayanthal P and Pollak F H 1984 *Phys. Rev. Lett.* **52** 1822
[24] Lin L Y, Chang C W, Chen W H, Chen Y F, Guo S P and Tamargo M C 2004 *Phys. Rev.* B **69** 075204
[25] Kaschner A, Haboeck U, Strassburg M, Kaczmarczky G, Hoffmann A, Thomsen C, Zeuner A, Alves H R, Hoffmann D M and Meyer B K 2002 *Appl. Phys. Lett.* **80** 1909
[26] Du G, Ma Y, Zhang Y and Yang T 2005 *Appl. Phys. Lett.* **87** 213103
[27] Xu H Y, Liu Y C, Xu C S, Shao C L and Mu R 2006 *J. Chem. Phys.* **124** 074707
[28] Islam Md N, Pradhan A and Kumar S 2005 *J. Appl. Phys.* **98** 024309
[29] Lin K F, Cheng H M, Hsu H C and Hsieh W F 2006 *Appl. Phys. Lett.* **88** 263117
[30] Cheng H M, Lin K F, Hsu H C, Lin C J, Lin L J and Hsieh W F 2005 *J. Phys. Chem.* B **109** 18385
[31] Lin K F, Cheng H M, Hsu H C, Lin L J and Hsieh W F 2005 *Chem. Phys. Lett.* **409** 208